Supporting Information

Realizing Ultralow Lattice Thermal Conductivity in $CuInTe_2$ by Controlled Cation Disorder

Songlin Li,[†a,b] Jianxiang Zhai,[†a] Chenghao Xie,[a] Minghao Ye,[a] Guoqing Ding,[a] Junxi Mei,[a] Qingjie Zhang,[a] Xinfeng Tang,[a] and Gangjian Tan*[a,b]

[a] *State Key Laboratory of Advanced Technology for Materials Synthesis and Processing, Wuhan University of Technology, Wuhan 430070, China*

[b] *Hubei Longzhong Laboratory, Wuhan University of Technology Xiangyang Demonstration Zone, Xiangyang 441000, China*

[†]Songlin Li and Jianxiang Zhai contributed equally to this work.

[*]***Corresponding author:***

Gangjian Tan (gtan@whut.edu.cn).

1. Theoretical minimum lattice thermal conductivity calculation

The theoretical minimum lattice thermal conductivity of $(CuInTe_2)_{0.6}(2CdTe)_{0.4}$ was estimated using Cahill model,[1] which can be expressed as:[2,3]

$$\kappa_{\min} \approx 1.21 n^{\frac{2}{3}} k_B \frac{2v_t + v_l}{3} \quad (1)$$

where n is the number density of atoms, k_B is the Boltzmann constant, v_t and v_l are the transverse and longitudinal sound velocities , respectively. The parameter n was calculated from the lattice parameters of the unit cell. The transverse and longitudinal sound velocities were taken as v_t = 1590 m s^{-1} and v_l = 3043 m s^{-1}, respectively, as measured by the ultrasonic pulse–echo method and summarized in Table S7. Using the above parameters, the theoretical minimum lattice thermal conductivity of $(CuInTe_2)_{0.6}(2CdTe)_{0.4}$ was calculated to be 0.35 W m^{-1} K^{-1}.

2. Density and heat capacity

The density and heat capacity of all samples are summarized in Table S1. The density (ρ) was determined using the Archimedes method, while the heat capacity (C_p) was estimated based on the Dulong–Petit law.

Table S1. Heat capacity, density, and relative density of $(CuInTe_2)_{1-x}(2CdTe)_x$ (x = 0, 0.05, 0.1, 0.15, 0.2, 0.25, 0.3, 1/3, 0.4 and 0.5).

Samples	C_p (J g^{-1} K^{-1})	ρ (g cm^{-3})	Relative density (%)
x = 0	0.2301	6.034	99.8
x = 0.05	0.2289	5.923	98.0
x = 0.1	0.2277	6.027	99.7
x = 0.15	0.2265	5.993	99.4
x = 0.2	0.2253	5.967	99.1
x = 0.25	0.2241	5.989	99.9
x = 0.3	0.2229	5.858	97.8
x = 1/3	0.2222	5.932	99.2
x = 0.4	0.2207	5.887	98.6
x = 0.5	0.2184	5.869	98.6

3. Chemical potential spaces and defect formation energy

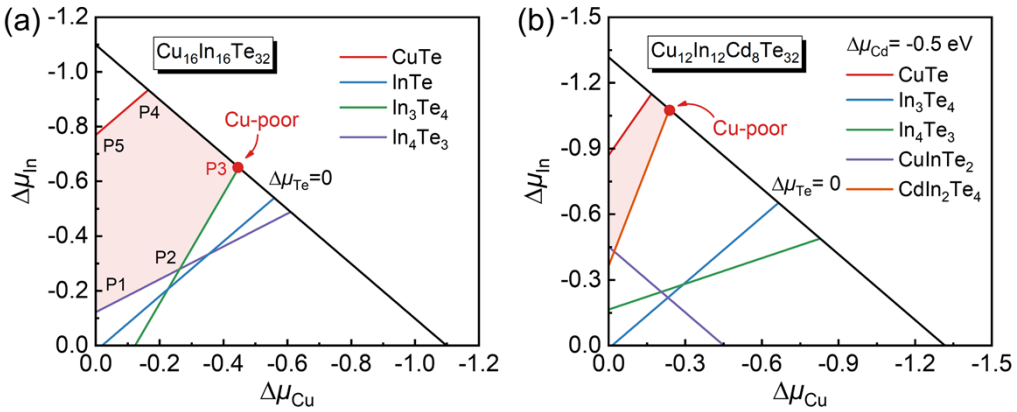

Fig. S1 The calculated stable chemical potential region of (a) $Cu_{16}In_{16}Te_{32}$ and (b) $Cu_{12}In_{12}Cd_8Te_{32}$.

The phase stability region of $Cu_{16}In_{16}Te_{32}$ and $Cu_{12}In_{12}Cd_8Te_{32}$, limited by the red area in Fig. S1, spans a large portion of the chemical potential space, plotted here as a

function of the chemical potentials of copper and indium. As $Cu_{16}In_{16}Te_{32}$, the boundaries of $\Delta\mu_i$ ($\Delta\mu_i$[poorest-i, richest-i]) for Cu and In are $\Delta\mu_{Cu}$[−0.45, 0.00] eV, $\Delta\mu_{In}$[−0.93, −0.12] eV, respectively. As $Cu_{12}In_{12}Cd_8Te_{32}$, corresponding Cu, In and Cd are $\Delta\mu_{Cu}$[−0.24, 0.00] eV, $\Delta\mu_{In}$[−1.15, −0.43] eV and $\Delta\mu_{Cd}$ = −0.5eV, respectively. Such differences in atomic chemical potentials lead to distinct formation energies. The formation energies of different types of defects and their detailed comparisons are shown in Fig. S2.

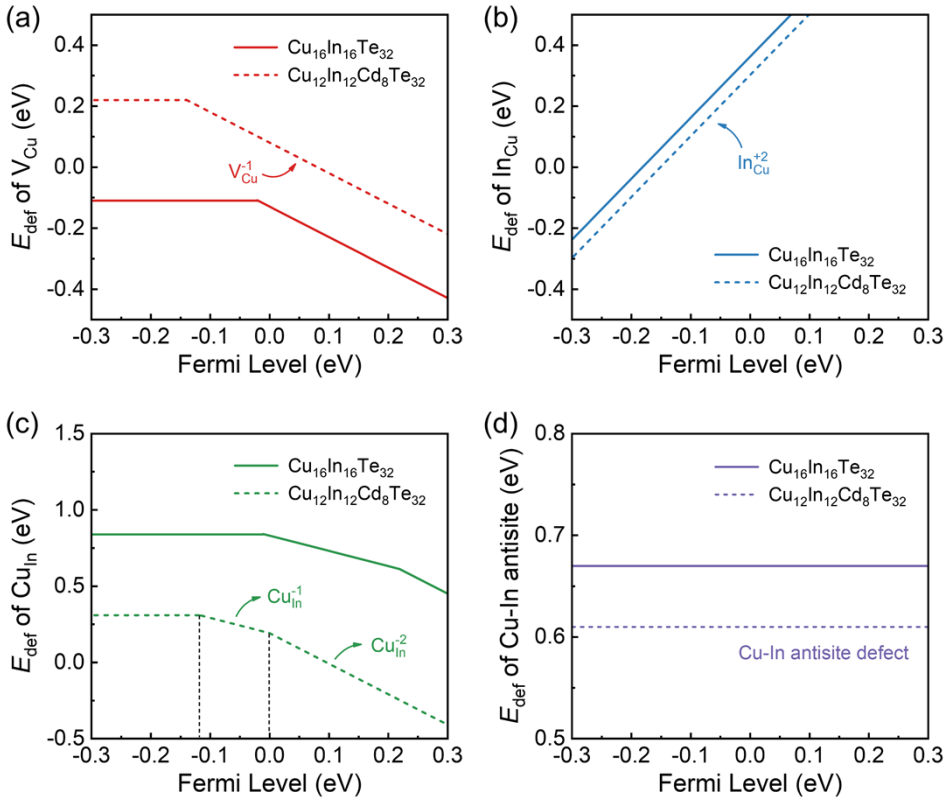

Fig. S2 Comparison of defect formation energies between $Cu_{16}In_{16}Te_{32}$ and $Cu_{12}In_{12}Cd_8Te_{32}$: (a) V_{Cu}, (b) In_{Cu}, (c) Cu_{In}, and (d) Cu–In antisite.

3. Elemental point analyses by electron probe X-ray microanalysis

By performing EPMA point analyses at different regions, the relative elemental compositions were obtained, as summarized in Table S2.

Table S2. EPMA point analysis data of the $(CuInTe_2)_{0.7}(2CdTe)_{0.3}$ sample.

Positions	Elements	Weight (%)	Atomic (%)
Spot 1	Cu	9.01	16.02
	Cd	15.46	15.54
	In	16.21	15.94
	Te	59.32	52.51
Spot 2	Cu	8.57	15.28
	Cd	15.75	15.88
	In	15.97	15.77
	Te	59.72	53.06

4. Rietveld refinements

The XRD patterns of all $(CuInTe_2)_{1-x}(2CdTe)_x$ compositions were analyzed through Rietveld refinement, and the results are presented in Figs. S3–S5. Samples with $x < 0.2$ were refined using a tetragonal structural model, whereas those with $x > 0.2$ were fitted using a cubic model. Notably, for the composition with $x = 0.25$, both structural models were employed to further verify the occurrence of a structural transition.

For the CdTe-alloyed compositions exhibiting a tetragonal structure, Cu–In cation intermixing was introduced into the refinement model to gain deeper insight into the evolution of cation disorder. Based on this model, the chemical occupancies at distinct cation sites (site occupancy factor, SOF) corresponding to the 4a and 4b sites, were constrained as follows:

$$SOF_{4a}\,(Cu) + SOF_{4a}\,(Cd) + SOF_{4a}\,(In) = 1 \quad (1)$$

$$SOF_{4b}\,(Cu) + SOF_{4b}\,(Cd) + SOF_{4b}\,(In) = 1 \quad (2)$$

The structural parameters from Rietveld refinement are summarized in Table S2-S8. The atomic occupancy (Occ) is calculated as SOF by the site multiplicity, the latter of which can be normalised to the multiplicity of the general potition of the group.

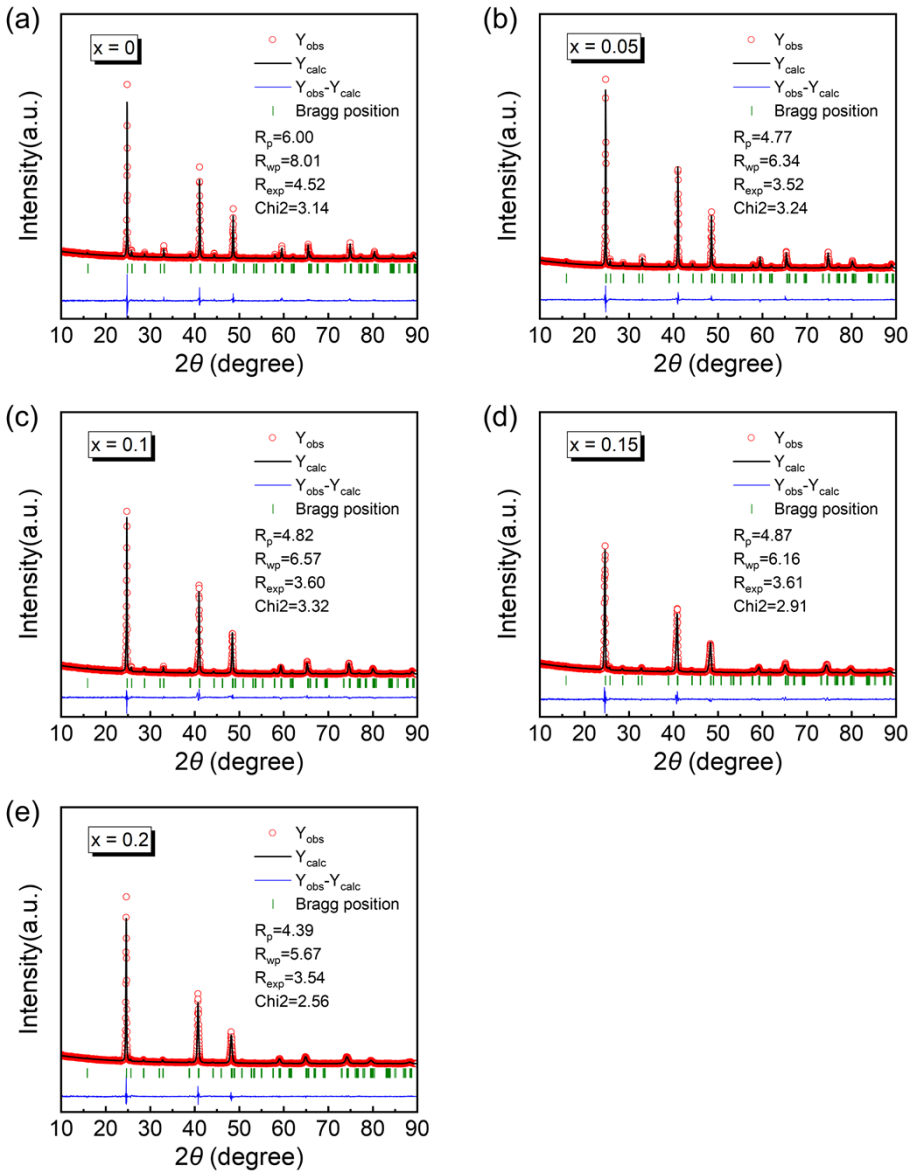

Fig. S3 The Rietveld refinement analysis for tetragonal structural $(CuInTe_2)_{1-x}(2CdTe)_x$ ($x = 0$, 0.05, 0.1, 0.15, and 0.2) samples. The experimental data (Y_{obs}), calculated pattern (Y_{calc}), the difference curve (Y_{obs}-Y_{calc}) and expected Bragg position are shown as red circles, a black solid line, a blue solid line and green vertical ticks, respectively.

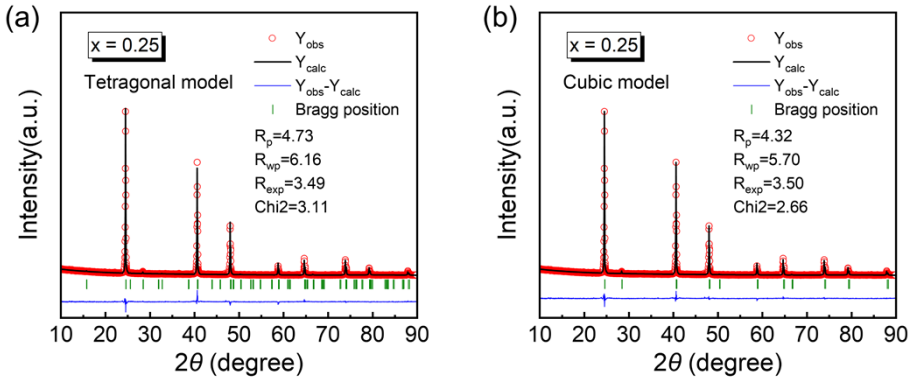

Fig. S4 The Rietveld refinement analysis for $(CuInTe_2)_{0.75}(2CdTe)_{0.25}$ sample: (a) tetragonal structural model and (b) cubic structural model.

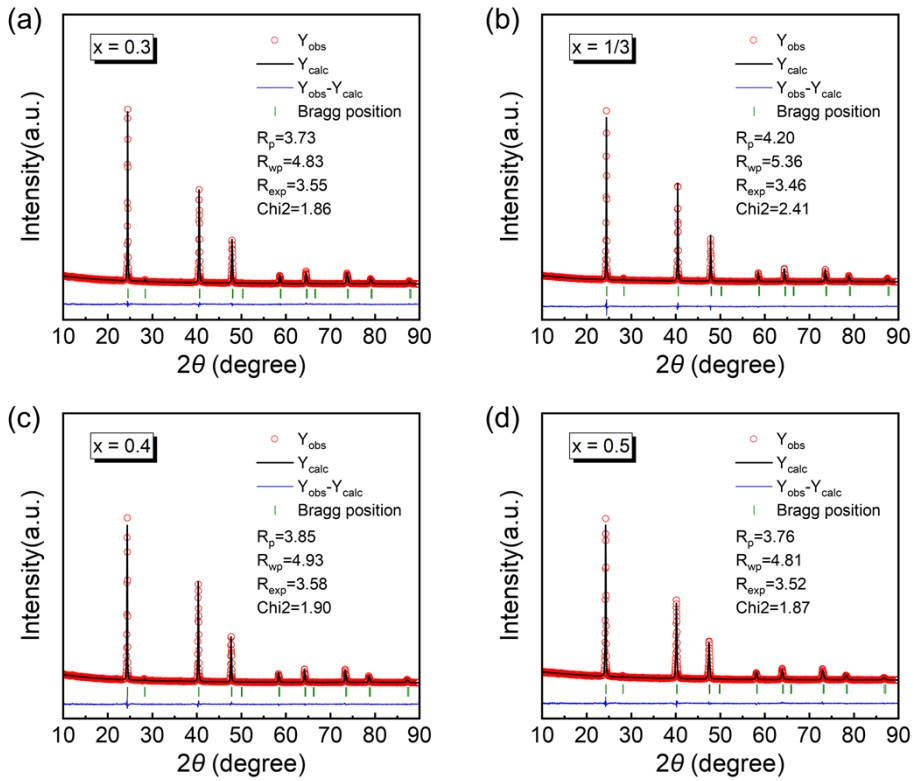

Fig. S5 The Rietveld refinement analysis for cubic structural $(CuInTe_2)_{1-x}(2CdTe)_x$ (x = 0.3, 1/3, 0.4 and 0.5) samples.

Table S3. The structural parameters (Positions, Biso, Occ and SOF) of $CuInTe_2$ from Rietveld refinement based on tetragonal structural model.

Wyckoff site	Fractional coordinates			Atom	Occ	SOF	Biso
	x	*y*	*z*				
4a	0	0	0	Cu	0.25	1	0.80355
4b	0	0	0.5	In	0.25	1	0.11893
8d	0.22032	0.25	0.125	Te	0.5	1	0.05683

Table S4. The structural parameters (Wyckoff site, Fractional coordinates, Occ, SOF and Biso) of $(CuInTe_2)_{0.95}(2CdTe)_{0.05}$ from Rietveld refinement based on tetragonal structural model.

Wyckoff site	Fractional coordinates			Atom	Occ	SOF	Biso
	x	*y*	*z*				
4a	0	0	0	Cu1	0.2288	0.9152	2.15936
				Cd1	0.0125	0.0500	
				In1	0.0087	0.0348	
4b	0	0	0.5	Cu2	0.0087	0.0348	0.98586
				Cd2	0.0125	0.05	
				In2	0.2288	0.9152	
8d	0.22435	0.25	0.125	Te1	0.5	1	0.78227

Table S5. The structural parameters (Wyckoff site, Fractional coordinates, Occ, SOF and Biso) of $(CuInTe_2)_{0.9}(2CdTe)_{0.1}$ from Rietveld refinement based on tetragonal structural model.

Wyckoff site	Fractional coordinates			Atom	Occ	SOF	Biso
	x	*y*	*z*				
4a	0	0	0	Cu1	0.2119	0.8474	2.30578
				Cd1	0.0250	0.1000	
				In1	0.0132	0.0526	
4b	0	0	0.5	Cu2	0.0132	0.0526	0.76214
				Cd2	0.0250	0.1000	
				In2	0.2119	0.8474	
8d	0.22592	0.25	0.125	Te1	0.5	1	0.71209

Table S6. The structural parameters (Wyckoff site, Fractional coordinates, Occ, SOF and Biso) of $(CuInTe_2)_{0.85}(2CdTe)_{0.15}$ from Rietveld refinement based on tetragonal structural model.

Wyckoff site	Fractional coordinates			Atom	Occ	SOF	Biso
	x	*y*	*z*				
4a	0	0	0	Cu1	0.1961	0.7842	1.45788
				Cd1	0.0375	0.1500	
				In1	0.0165	0.0658	
4b	0	0	0.5	Cu2	0.0165	0.0658	1.06670
				Cd2	0.0375	0.1500	
				In2	0.1961	0.7842	
8d	0.22842	0.25	0.125	Te1	0.5	1	0.78097

Table S7. The structural parameters (Wyckoff site, Fractional coordinates, Occ, SOF and Biso) of $(CuInTe_2)_{0.8}(2CdTe)_{0.2}$ from Rietveld refinement based on tetragonal structural model.

Wyckoff site	Fractional coordinates			Atom	Occ	SOF	Biso
	x	*y*	*z*				
4a	0	0	0	Cu1	0.1795	0.7181	0.60550
				Cd1	0.0500	0.2000	
				In1	0.0205	0.0819	
4b	0	0	0.5	Cu2	0.0205	0.0819	1.24831
				Cd2	0.0500	0.2000	
				In2	0.1795	0.7181	
8d	0.23287	0.25	0.125	Te1	0.5	1	1.17604

Table S8. The structural parameters (Wyckoff site, Fractional coordinates, Occ, SOF and Biso) of $(CuInTe_2)_{0.75}(2CdTe)_{0.25}$ from Rietveld refinement based on tetragonal structural model.

Wyckoff site	Fractional coordinates			Atom	Occ	SOF	Biso
	x	*y*	*z*				
4a	0	0	0	Cu1	0.1058	0.4231	1.34284
				Cd1	0.0625	0.2500	
				In1	0.0817	0.3269	
4b	0	0	0.5	Cu2	0.0817	0.3269	3.84280
				Cd2	0.0625	0.2500	
				In2	0.1058	0.4231	
8d	0.24545	0.25	0.125	Te1	0.5	1	1.52045

Table S9. The structural parameters (Wyckoff site, Fractional coordinates, Occ, SOF and Biso) of $(CuInTe_2)_{1-x}(2CdTe)_x$ (x = 0.25, 0.3, 1/3, 0.4 and 0.5) from Rietveld refinement based on cubic structural model.

Samples	Wyckoff site	Fractional coordinates			Atom	Occ	SOF	Biso
		x	*y*	*z*				
x = 0.25	4a	0	0	0	Cu1	0.0156	0.3750	1.83751
					Cd1	0.0104	0.2500	
					In1	0.0156	0.3750	
	4c	0.25	0.25	0.25	Te1	0.0417	1	1.81313
x = 0.3	4a	0	0	0	Cu1	0.0146	0.3500	1.91178
					Cd1	0.0125	0.3000	
					In1	0.0146	0.3500	
	4c	0.25	0.25	0.25	Te1	0.0417	1	1.53643
x = 1/3	4a	0	0	0	Cu1	0.0139	0.3333	1.93092
					Cd1	0.0139	0.3333	
					In1	0.0139	0.3333	
	4c	0.25	0.25	0.25	Te1	0.0417	1	1.82145
x = 0.4	4a	0	0	0	Cu1	0.0125	0.3000	1.52329
					Cd1	0.0167	0.4000	
					In1	0.0125	0.3000	
	4c	0.25	0.25	0.25	Te1	0.0417	1	1.06067
x = 0.5	4a	0	0	0	Cu1	0.0104	0.2500	1.66267
					Cd1	0.0208	0.5000	
					In1	0.0104	0.2500	
	4c	0.25	0.25	0.25	Te1	0.0417	1	1.24638

5. Tetragonal distortion parameter η

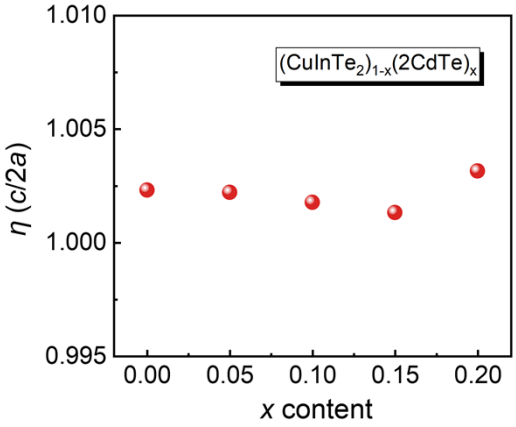

Fig. S6 CdTe content dependence of tetragonal distortion parameters for $(CuInTe_2)_{1-x}(2CdTe)_x$ (x = 0, 0.05, 0.1, 0.15, 0.2) samples.

6. Thermal conductivity

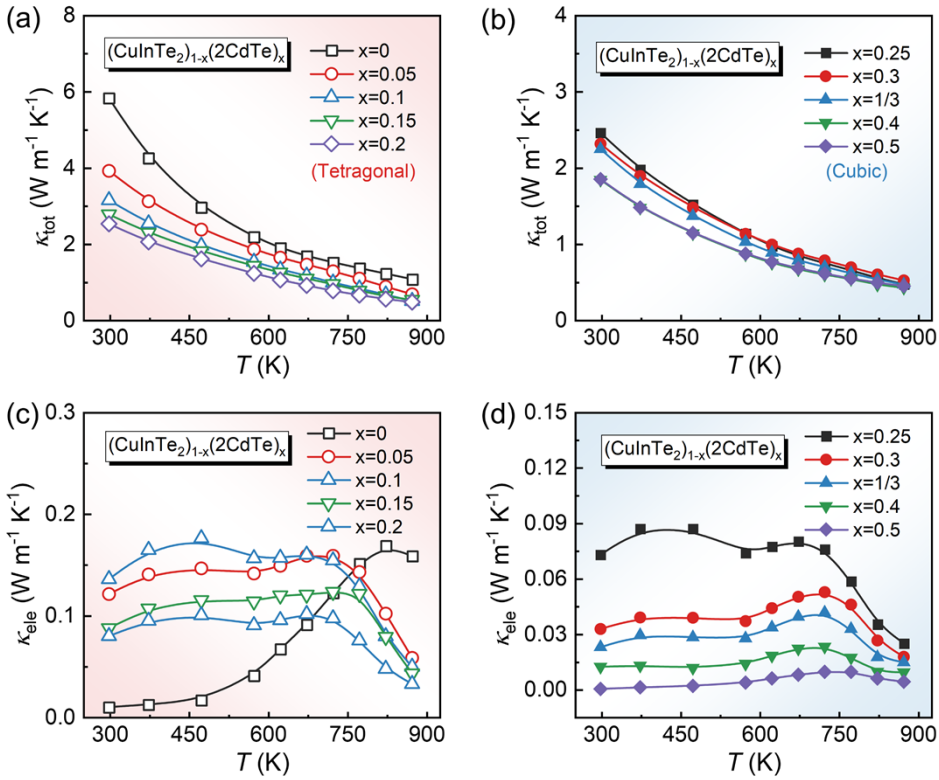

Fig. S7 Thermal transport properties of $(CuInTe_2)_{1-x}(2CdTe)_x$ samples. (a) and (c) illustrate the total thermal conductivity and electronic thermal conductivity for tetragonal samples ($x \leq 0.2$), while (b) and (d) show the corresponding properties for cubic samples ($x > 0.2$).

7. Callaway–Klemens model fitting of lattice thermal conductivity and elastic parameters

Based on the Callaway and Klemens models, the effects of Cd substitution and Cu-In antisite defects on the thermal conductivity of tetragonal structural $(CuInTe_2)_{1-x}(2CdTe)_x$ were evaluated in terms of mass fluctuation and strain field fluctuation, as shown in Fig. S8.

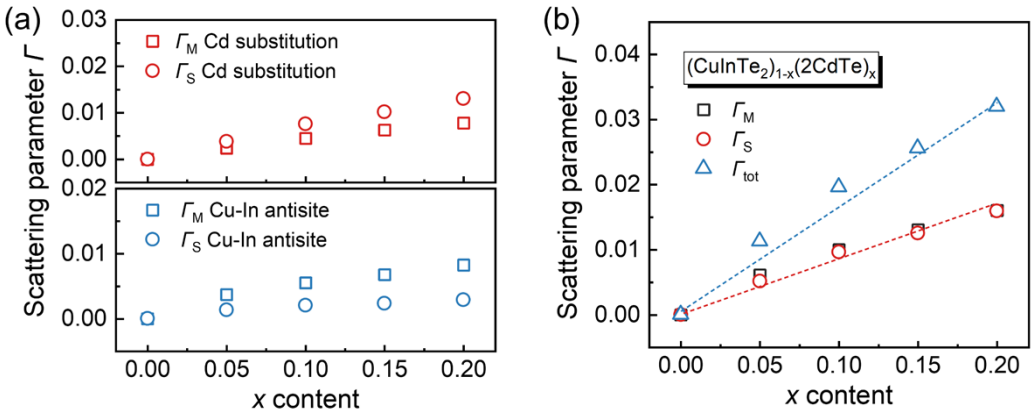

Fig. S8 (a) Mass and strain field fluctuations caused individually by Cd substitution and Cu–In antisite defects as a function of CdTe content. (b) Scattering parameter as a function of CdTe content.

Under this model, assuming the phonon scattering mechanisms governing heat transport are Umklapp processes and point defect scattering, the lattice thermal conductivity of the disordered $(CuInTe_2)_{1-x}(2CdTe)_x$ (κ_{lat}) with respect to that of parent compound (κ_{lat}^{pure}) is given by:[4,5]

$$\frac{\kappa_{lat}}{\kappa_{lat}^{pure}} = \frac{\tan^{-1} u}{u} \tag{3}$$

where u is the disorder scaling parameter that can be expressed as:

$$u^2 = \frac{\pi^2 \theta_D \Omega}{h v_s} \kappa_{lat}^{pure} \Gamma \tag{4}$$

where Ω is the average atomic volume, h stands for Planck constant, v_s is the average sound velocity, θ_D represents the Debye temperature and they can be calculate by the equation as:[6]

$$v_{\mathrm{s}}=\left[\frac{1}{3}\left(\frac{1}{v_{\mathrm{l}}^{3}}+\frac{2}{v_{\mathrm{t}}^{3}}\right)\right]^{-\frac{1}{3}} \tag{5}$$

$$\theta_{\mathrm{D}}=\left[\frac{hv_{\mathrm{s}}}{k_{\mathrm{B}}}\left(\frac{3N}{4\pi V}\right)\right]^{\frac{1}{3}} \tag{6}$$

where k_{B} is Boltzmann constant, V is the volume in a unit cell and N is the number of atoms in the unit cell. The Γ is the scattering parameter due to mass fluctuations and strain field fluctuations, respectively. The scattering parameter can be calculated by the model of Slack[7] and Abeles[8]:

$$\Gamma=\Gamma_{\mathrm{M}}+\Gamma_{\mathrm{S}} \tag{7}$$

where Γ_{M} and Γ_{S} are scattering parameters related to mass fluctuation and strain field fluctuation, respectively. They can be expressed as:

$$\Gamma_{\mathrm{M}}=\frac{\sum_{i=1}^{n}c_i\left(\frac{\overline{M_i}}{\overline{\overline{M}}}\right)^{2}f_i^{1}f_i^{2}\left(\frac{M_i^{1}-M_i^{2}}{\overline{M_i}}\right)^{2}}{\sum_{i=1}^{n}c_i} \tag{8}$$

$$\Gamma_{\mathrm{S}}=\frac{\sum_{i=1}^{n}c_i\left(\frac{\overline{M_i}}{\overline{\overline{M}}}\right)^{2}f_i^{1}f_i^{2}\varepsilon_i\left(\frac{r_i^{1}-r_i^{2}}{\overline{r_i}}\right)^{2}}{\sum_{i=1}^{n}c_i} \tag{9}$$

where n is the number of different crystallographic sublattice types in the lattice, c_i is the degeneracy of the i^{th} atomic occupation, $\overline{M_i}$ and $\overline{r_i}$ are the average mass and covalent radius of atoms at the i^{th} atomic site. $\overline{\overline{M}}$ is the average relative atomic mass, f_i^k, M_i^k and r_i^k are the occupied fraction, atomic mass and radius of the k^{th} atom at the i^{th} atomic site, respectively. The relations discussed above can be expressed as:

$$\overline{M_i}=\sum_k f_i^k M_i^k \tag{10}$$

$$\overline{r_i}=\sum_k f_i^k r_i^k \tag{11}$$

$$\overline{\overline{M}} = \frac{\sum_{i=1}^{n} c_i \overline{M_i}}{\sum_{i=1}^{n} c_i} \tag{12}$$

The parameter ε is related to the Grüneisen parameter γ and elastic properties, which can be obtained by:[9–11]

$$\varepsilon = \frac{2}{9}\left(6.4\gamma \frac{1+v_{\mathrm{p}}}{1-v_{\mathrm{p}}}\right)^2 \tag{13}$$

$$\gamma = \frac{3}{2}\left(\frac{1+v_{\mathrm{p}}}{2-3v_{\mathrm{p}}}\right) \tag{14}$$

where v_{p} is the Poisson ratio, which can be calculated from v_{l} and v_{t} as follows:

$$v_{\mathrm{p}} = \frac{1-2\left(\frac{v_{\mathrm{t}}}{v_{\mathrm{l}}}\right)^2}{2-2\left(\frac{v_{\mathrm{t}}}{v_{\mathrm{l}}}\right)^2} \tag{15}$$

Correspondingly, the results of the sound velocity measurements and the related elastic parameters are summarized in Table S10.

Table S10. Sound velocity and elastic properties of $(CuInTe_2)_{1-x}(2CdTe)_x$ (x = 0, 0.05, 0.1, 0.15, 0.2, 0.25, 0.3, 1/3, 0.4 and 0.5)

Samples	v_l (m s^{-1})	v_t (m s^{-1})	v_s (m s^{-1})	v_p	γ	θ_D (K)
x = 0	3512	1827	2044	0.315	1.87	196
x = 0.05	3436	1789	2002	0.314	1.86	192
x = 0.1	3394	1764	1974	0.315	1.87	189
x = 0.15	3333	1758	1965	0.307	1.82	188
x = 0.2	3289	1739	1943	0.306	1.81	185
x = 0.25	3227	1707	1908	0.306	1.81	181
x = 0.3	3175	1671	1869	0.308	1.83	177
x = 1/3	3117	1637	1830	0.310	1.83	173
x = 0.4	3043	1590	1779	0.312	1.85	168
x = 0.5	2953	1539	1722	0.314	1.86	162

8. Vickers hardness

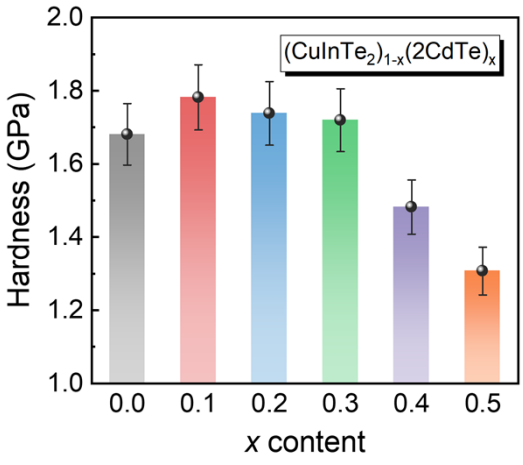

Fig. S9 Vickers hardness of $(CuInTe_2)_{1-x}(2CdTe)_x$ (x = 0, 0.1, 0.2, 0.3, 0.4, 0.5) samples measured at room temperature.

References

1 D. G. Cahill, S. K. Watson and R. O. Pohl, *Phys. Rev. B*, 1992, **46**, 6131–6140.

2 T. Xing, C. Zhu, Q. Song, H. Huang, J. Xiao, D. Ren, M. Shi, P. Qiu, X. Shi, F. Xu and L. Chen, *Adv. Mater.*, 2021, **33**, 2008773.

3 Y. Shi, N. Mashmoushi, W. Wegner, P. Jafarzadeh, Z. Sepahi, A. Assoud and H. Kleinke, *J. Mater. Chem. C*, 2019, **7**, 8029–8036.

4 H. Wang, A. D. LaLonde, Y. Pei and G. J. Snyder, *Adv. Funct. Mater.*, 2013, **23**, 1586–1596.

5 J. Yang, G. P. Meisner and L. Chen, *Appl. Phys. Lett.*, 2004, **85**, 1140–1142.

6 T. J. Zhu, S. N. Zhang, S. H. Yang and X. B. Zhao, *Phys. Status Solidi RRL – Rapid Res. Lett.*, 2010, **4**, 317–319.

7 G. A. Slack, *Phys. Rev.*, 1957, **105**, 829–831.

8 B. Abeles, *Phys. Rev.*, 1963, **131**, 1906–1911.

9 Y. Pei, C. Chang, Z. Wang, M. Yin, M. Wu, G. Tan, H. Wu, Y. Chen, L. Zheng, S. Gong, T. Zhu, X. Zhao, L. Huang, J. He, M. G. Kanatzidis and L.-D. Zhao, *J. Am. Chem. Soc.*, 2016, **138**, 16364–16371.

10 D. S. Sanditov and V. N. Belomestnykh, *Tech. Phys.*, 2011, **56**, 1619–1623.

11 Q. Xiong, Y. Yan, N. Li, B. Zhang, S. Zheng, Y. Feng, G. Wang, H. Liao, Z. Huang, J. Li, G. Wang, X. Lu and X. Zhou, *Appl. Phys. Lett.*, 2022, **121**, 013903.